Supporting Information

Tadenev et al. 10.1073/pnas.1016531108

SI Methods

Immunofluorescence. Eyes were harvested from *Bbs8* mice and fixed in 4% paraformaldehyde. Twenty-micrometer cryosections were cut and stained with rhodopsin antibody (rabbit, 1:1,000; polyclonal directed against the N-terminal 20 amino acids of bovine rhodopsin) and counterstained with DAPI.

Hematoxylin/Eosin Staining. Mice were perfused with 4% paraformaldehyde and kidneys were embedded in paraffin and sectioned. Hematoxylin/eosin staining was performed using standard techniques.

Quantitative PCR. RNA was harvested using the standard TRIzol (Invitrogen) protocol. First-strand cDNA was synthesized (Invitrogen) and quantitative PCR was performed using SYBR green reagents (Qiagen) and an ABI StepOnePlus machine with specific primers to amplify GAPDH and *Bbs8* mRNA. *Bbs8* was normalized to GAPDH, and arbitrary expression units were determined by ΔΔCt method.

Western Blot. Tissues were homogenized in Laemmli sample buffer and the resulting lysates were separated on a polyacrylamide gel and transferred to PVDF membrane using standard protocols. Blot was probed with anti-GFP antibody (Invitrogen).

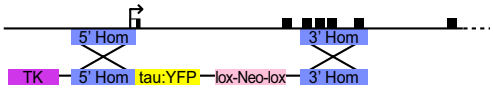

Fig. S1. Schematic of BBS-targeting construct. The *Bbs8* coding exons are indicated by black boxes and the transcription start site by an arrow. Homology arms (blue) were cloned from mouse 129/Sv BACs (Research Genetics). Targeting constructs were assembled in a pBC plasmid with a modified polylinker and various cassettes. The thymidine kinase gene for counterselection (TK, purple), the tau:YFP reporter protein (yellow), and lox-pgkNeo-lox (pink) (1) were previously described. At the *Bbs8* locus, construct insertion maintained upstream regulatory elements but deleted 15.8 kb, including the start codon and first two exons. The tau:YFP reporter was integrated precisely at the BBS8 start codon and was followed by the SV40 polyadenylation site to ensure transcript termination. 129/Sv ES cells (The Johns Hopkins University Transgenic Core) were electroporated and underwent double selection with G418 and ganciclovir. Clones were screened by Southern blot using an adjacent probe and positive clones injected into blastocysts. Germline transmission was achieved, and breeding was maintained from the descendants of a single clone per line with genotyping performed by PCR. The lox-Neo-lox cassette was removed by breeding to Cre-expressing mice.

1. Zhao H, Reed RR (2001) X inactivation of the OCNC1 channel gene reveals a role for activity-dependent competition in the olfactory system. *Cell* 104:651–660.

A.

$BBS8^{+/+}$	$BBS8^{+/-}$	$BBS8^{-/-}$	total
41	74	19	134

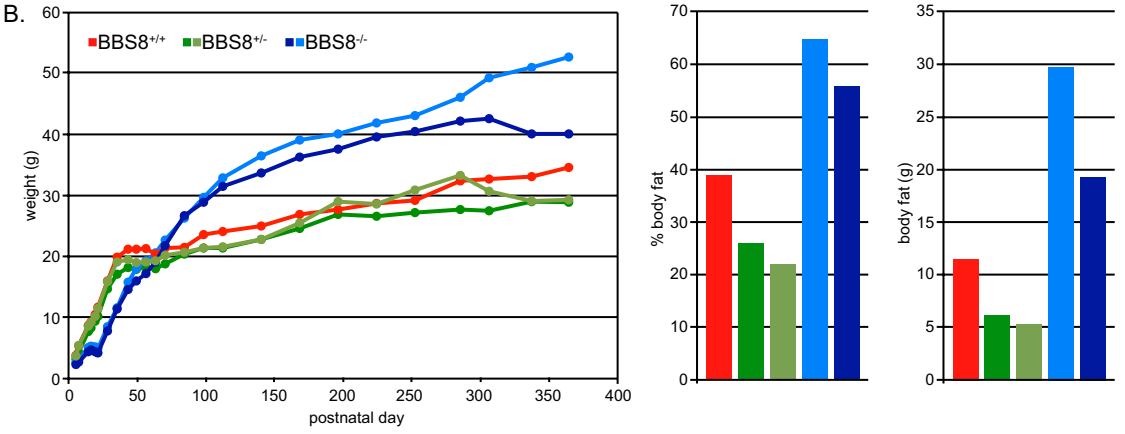

Fig. S2. Survival and weight of $Bbs8^{-/-}$ mice. (*A*) Distribution of genotypes of progeny from heterozygous mating pairs at PD21. (*B*) Weight gain in $Bbs8^{+/+}$, $Bbs8^{+/-}$, and $Bbs8^{-/-}$ female littermates (*Left*). Bar graphs of the same animals showing the percentage body fat by weight and total body fat determined by EchoMRI scan of 1-y-old mice (*Right* panels).

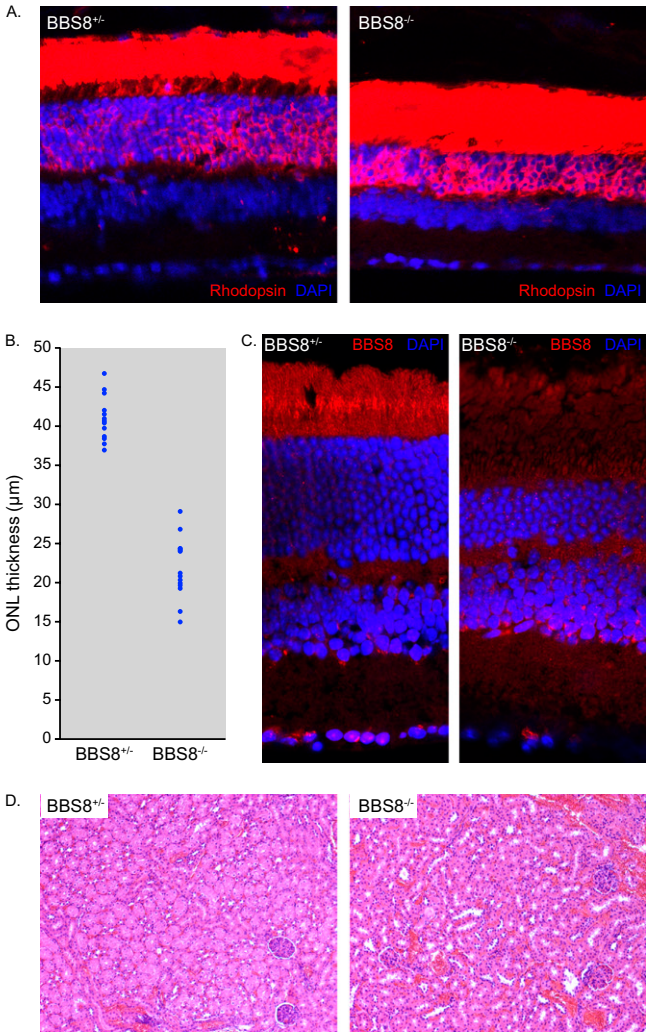

Fig. S3. Retinal degeneration and renal anomalies in *Bbs8*$^{-/-}$ mice. (*A*) Retinal sections from adult *Bbs8*$^{+/-}$ and *Bbs8*$^{-/-}$ mice were immunostained for rhodopsin and counterstained with DAPI. A dramatic thinning of the outer nuclear layer (ONL) is apparent in mutant tissue. (*B*) ONL thickness was measured from $n = 2$ mice/genotype. Sections from various regions were used, and at least four measurements were taken per animal. The ONL is significantly thinner in the mutant ($P < 0.001$). (*C*) Retinal sections from *Bbs8*$^{+/-}$ and *Bbs8*$^{-/-}$ mice stained with anti-BBS8 antibodies. Signal is observed within the connecting cilium region of the photoreceptor outer segments of heterozygous animals; no signal is detected in null mice. (*D*) Loss of BBS8 results in mild tubular dilation in the deep cortex of the kidney. Sections from 8-mo-old *Bbs8*$^{+/-}$ and *Bbs8*$^{-/-}$ mice were stained with hematoxylin and eosin and imaged by bright-field microscopy.

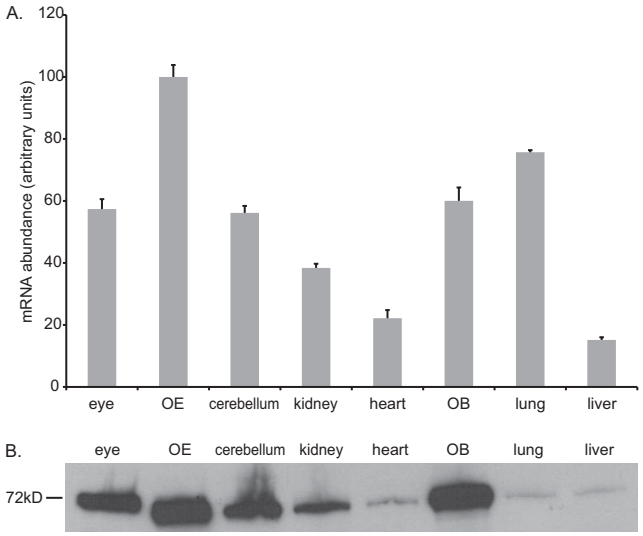

Fig. S4. Expression of BBS8 in various tissues. (*A*) Quantitative PCR for *Bbs8* mRNA performed on the indicated tissues from an adult WT animal. (*B*) Anti-GFP Western blot of protein lysates from indicated tissues harvested from an adult $Bbs8^{+/-}$ animal. The predicted molecular weight of tau:YFP is 67 kDa.

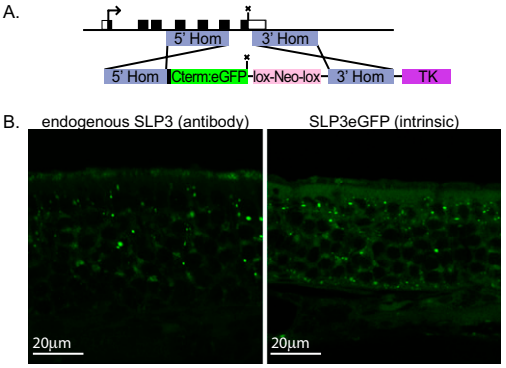

Fig. S5. Generation of SLP3:eGFP mice. (*A*) Schematic for the targeting strategy used to create the SLP3:eGFP mouse. The SLP3-targeting construct was assembled using the same methods and cassettes as described for *Bbs8* with the exception of an eGFP fusion protein cassette (Clontech). The reporter construct was integrated at the 3′ end of the SLP3 gene such that 109 bp of the penultimate exon, the entire final intron (1.9 kb), and 790 bp of the final exon (including 225 bp of coding sequence) were eliminated and the coding sequence from those exons (334 bp total) was replaced as a SLP3 cDNA segment. The segment was immediately followed by the eGFP ORF so that the entire SLP3 gene would be transcribed as a translational fusion to eGFP. The eGFP sequence replaced the SLP3 stop codon and 3′ sequences and was followed by an SV40 polyadenylation addition sequence. The SLP3 coding sequence (black boxes), untranslated regions (white boxes), transcription start (arrow), and translation stop (x) are indicated. (*B*) SLP3:eGFP localization mimics that of endogenous SLP3. (*Left*) Endogenous SLP3 in WT OE detected by an antibody against SLP3. (*Right*) Intrinsic fluorescence in the OE of the SLP3:eGFP mouse. Each image represents a single confocal plane; this accounts for the minor differences in apparent SLP3:eGFP distribution with Fig. 3*C* (flattened Z-stacks).

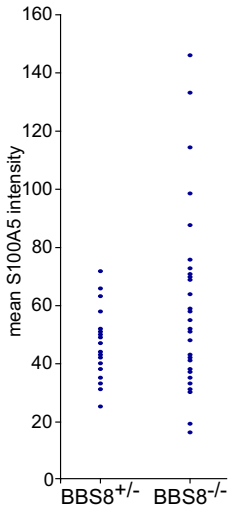

Fig. S6. ORI7-expressing *Bbs8*$^{-/-}$ OSNs display increased variability in S100A5 protein expression. Sections of olfactory epithelium from *Bbs8*$^{+/-}$ and *Bbs8*$^{-/-}$ were immunostained for ORI7 and S100A5, and the mean pixel intensity for S100A5 was determined within the cell body of ORI7-positive olfactory sensory neurons (OSNs). Mean S100A5 fluorescence was higher (59.9 vs. 46.1, $P < 0.05$) and more variable (975.77 vs. 115.59, $P < 0.001$) in mutant OSNs compared with controls. $n = 27$ for *Bbs8*$^{+/-}$; $n = 30$ for *Bbs8*$^{-/-}$. It should be noted that the S100A5 levels in ORI7-expressing OSNs cannot be directly compared with those from M72-expressing OSNs (Fig. 6) as different acquisition settings were required for the two experimental conditions. In addition, unlike in the M72 experiment, S100A5 levels were not normalized to ORI7 intensity because olfactory receptor (OR) protein mislocalizes in mutant OSNs (Fig. 3 *B* and *C*). This, in combination with the lack of proof that the ORI7 protein labels only a single OR species, represents a significant limitation to performing this experiment with OR-directed antibodies rather than OR-reporter mice.

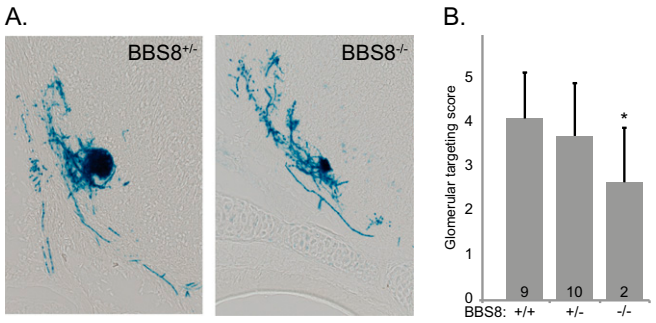

Fig. S7. Loss of BBS8 adversely affects glomerular formation in neonatal pups. (*A*) (*Left*) X-Gal–stained section through a medial P2 glomerulus from a *Bbs8*$^{+/+}$; *P2*$^{+/TL}$ PD1 mouse reveals a tight convergence of axons. (*Right*) Section from the same region of a *Bbs8*$^{-/-}$;*P2*$^{+/TL}$ littermate shows reduced axonal convergence. (*B*) Glomerular targeting efficiency was quantified by using a 0–5 scale, where 0 represented no axonal convergence and 5 represented convergence to a single, tightly circumscribed glomerulus. Scorers were blind to genotype and instructed not to take into account the number or intensity of stained fibers. Scores were averaged for each genotype; error bars represent SD, and numbers within the bars indicate the number of glomeruli scored. *$P < 0.01$ vs. *Bbs8*$^{+/+}$.